

J. THIÉBAUD  
C. FITTSCHEN 

# Near infrared cw-CRDS coupled to laser photolysis: Spectroscopy and kinetics of the HO<sub>2</sub> radical

Laboratoire de Physico-Chimie des Processus de Combustion et de l'Atmosphère, PC2A UMR 8522, Université des Sciences et Technologies de Lille, 59655 Villeneuve d'Ascq Cedex, France

Received: 31 March 2006/Revised version: 26 April 2006  
Published online: 23 June 2006 • © Springer-Verlag 2006

**ABSTRACT** We present in this work a new experimental set-up for sensitive detection of reactive species: continuous wave cavity ring-down spectroscopy (cw-CRDS) as a detection method in laser photolysis reactor. HO<sub>2</sub> radicals were generated by using a 248 nm photolysis of SOCl<sub>2</sub>/CH<sub>3</sub>OH/O<sub>2</sub> mixtures and were detected in the first vibrational overtone of the OH stretch around 6625 cm<sup>-1</sup>, using a DFB diode laser. In order to perform the spectroscopic and kinetic measurements of the HO<sub>2</sub> radical, two different timing schemes have been used. The absorption line strength of the transition at 6625.784 cm<sup>-1</sup> has been extracted from kinetic measurement to  $(5.2 \pm 1.0) \times 10^{-21}$  cm<sup>2</sup> molecule<sup>-1</sup>cm<sup>-1</sup>. The detection limit for the actual set-up is  $2 \times 10^{12}$  molecules cm<sup>-3</sup>.

PACS 42.62.Fi; 82.33.Tb; 82.20.W


## 1 Introduction

The HO<sub>2</sub> radical plays a central role in atmospheric chemistry because it is closely coupled to the OH radical and it has an important influence on the atmospheric oxidizing capacity. Monitoring its concentration in the atmosphere or in laboratory experiments has long been a goal, but its short lifetime and consequently low concentration provided a serious challenge. The self-reaction of HO<sub>2</sub> is relatively fast [1–4] and the larger the initial HO<sub>2</sub> concentration, the faster the self-reaction. Therefore, the techniques used to study the HO<sub>2</sub> radical must present a suitable balance between sensitivity and time resolution. Because it achieves this requirement, the UV absorption spectroscopy has become a widely used technique to monitor the HO<sub>2</sub> radical and it has enabled important kinetic data to be obtained [3, 5–8]. However, the broad and structureless absorption of HO<sub>2</sub> in this wavelength range leads to many overlaps within the absorption features of other species like peroxy radicals. This lack of selectivity is an important limitation of the UV absorption spectroscopy that encouraged the development of spectroscopic measurements in the infrared region where we can find narrow and resolved absorption lines of small structures like the HO<sub>2</sub> radical [9–13]. Although the mid-infrared range provides enticing absorption cross-sections, it induces problems

like pressure induced line broadening or sampling issues. Peroxy radicals like HO<sub>2</sub> are known to have absorption bands in the near-IR region, a vibronic progression in the low-lying <sup>2</sup>A' ← <sup>2</sup>A'' transition (around 7017.5 cm<sup>-1</sup> for HO<sub>2</sub>), as well as the first vibrational overtone in the OH stretch (centered at 6648.9 cm<sup>-1</sup> for HO<sub>2</sub>). This wavelength range offers weaker line strengths than in the mid-IR but that can be balanced by taking advantage of higher working pressure before line broadening becomes a problem. Also more powerful, reliable and low cost devices (laser sources, detector, optics, etc) from the telecom industry are now available in this wavelength region. Several experiments have been reported using laser diode in the near-IR to detect HO<sub>2</sub> radicals: Taatjes and Oh [14] detected HO<sub>2</sub> by the 2ν<sub>1</sub> band at 6625.8 cm<sup>-1</sup> using wavelength modulation spectroscopy. Christensen et al. monitored HO<sub>2</sub> by the same overtone band at 6638.2 cm<sup>-1</sup> to study the kinetics of HO<sub>2</sub> + NO<sub>2</sub> [15] and the HO<sub>2</sub> self reaction [2]. Recently, Kanno et al. measured the nitrogen and water-pressure broadening coefficients of the HO<sub>2</sub> band at around 7020.8 cm<sup>-1</sup> [16] and the rate enhancement effect of water on HO<sub>2</sub> self-reaction [1] using two-tone frequency modulation (TTFM) absorption spectroscopy. These wavelengths (or frequency) modulation techniques improve the sensitivity by using a multipass configuration in order to increase the probe beam pathlength through the absorbing medium. To further decrease the detection limit, a heterodyne detection to extract the signal from small intensity change over the bandwidth of a narrow HO<sub>2</sub> absorption line is used. We report in this paper another absorption spectroscopy technique to monitor time-resolved HO<sub>2</sub> concentrations: the continuous wave cavity ring-down spectroscopy (cw-CRDS). CRDS experiments achieve their high sensitivity by positioning the sample in a cavity, made of two highly reflective mirrors. The light trapped between these mirrors propagates back and forth within the cavity leading to several kilometers of absorption pathlength. While pulsed CRDS has been used quite often in pump-probe experiments [17–24], application of the cw-version in this type of experiments are more sparse [25, 26], probably due to more demanding timing control.

## 2 Experimental

The experimental set-up is composed of three main components: the quasi-static reactor, the photolysis excimer laser and the cw-cavity ring-down spectrometer (see Fig. 1).

 Fax: +33320436977, E-mail: christa.fittschen@univ-lille1.fr

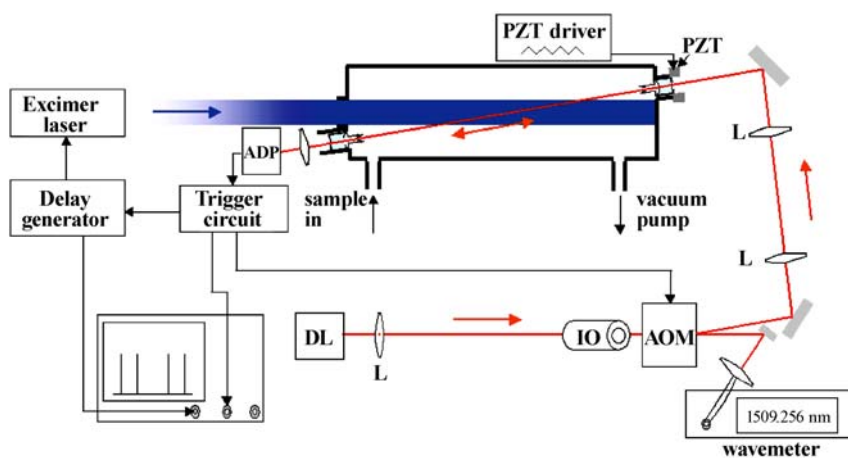


**FIGURE 1** Schematic of the experimental set-up. DL: diode laser, OI: optical isolator, AOM: acousto optic modulator, PZT: piezoelectric transducer, APD: avalanche photodiode, L: lens

## 2.1 The reactor

Initially constructed for a laser induced fluorescence experiment [27], the stainless steel flow cell was modified to enable the implementation of the cw-CRD spectrometer. Mechanical pieces were designed to hold the cavity mirrors at the extremities of each side of the flow cell permitting an accurate optical alignment: a mirror block was made to be enclosed in an  $X$ - $Y$ - $Z$  support (Newport U100-A Ultima series) on each side of the cell. In order to enable fine adjustments of the mirror position, this connection is pushed into a collar-like piece with a toric seals preventing the reactor from leaking. A gas inlet on the collar was inserted to admit a clean and dry helium flow in front of the mirrors in order to protect them from contamination due to the gas mixture. As the overlap between the probe beam and the photolysis beam must be maximized to get the best sensitivity, we designed a holding system for the mirror to make the distance between the cavity mirrors and the cell apertures defining the excimer pulse path as small as possible. This led to a  $4^\circ$  crossing angle for a cavity length  $L$  equal to 78 cm. The photolysis beam aperture consists of a quartz window of a diameter of 3 cm and is put on by pressure effect. Using the full width of the excimer beam (2.5 cm) and considering it perfectly collimated with no diffusion out of the photolysis volume, we calculated a maximal overlap of  $L_A = 37$  cm. The actual set-up uses a 2 cm quartz prism to guide the photolysis beam, which leads to an overlap of  $L_A = 30$  cm.

Five calibrated mass flow controllers (Tylan FC-260) are connected to the reactor to manage the gas mixture flow. A single-stage rotary pump and a pressure controller (Leybold-Heraeus MR 16) enables us to work at reduced pressure (between 10 and 100 Torr), monitored by a MKS Baratron pressure gauge (390HA-01000). Typical total gas flows are  $700 \text{ cm}^3 \text{ min}^{-1}$ , leading to a flow velocity within the reactor of  $7 \text{ cm s}^{-1}$  at 50 Torr. Spectroscopic measurements are performed in general with a repetition rate of 0.5 Hz, kinetic measurement are limited to 0.14 Hz, which is sufficient to replenish the reaction mixture between two laser shots.

## 2.2 The cavity ring-down spectrometer

Details on CRDS can be found in many reviews [28–31], only a brief description is given here. The

decay time of a cavity is extracted from the ring-down signal through

$$I(t) = I_0 \exp\left(-\frac{t}{\tau}\right), \quad (1)$$

where  $I(t)$  and  $I_0$  are the signals transmitted by the cavity. Measuring the decay time  $\tau_0$  of an empty cavity (in our case before the photolysis pulse) and the decay time  $\tau$  of the cavity containing the sample (i.e., after the photolysis pulse) permits the calculation of the absorption coefficient  $\alpha$  ( $\text{cm}^{-1}$ )

$$\alpha = [A] \times \sigma = \frac{R_L}{c} \left( \frac{1}{\tau} - \frac{1}{\tau_0} \right), \quad (2)$$

where  $R_L$  is the ratio between the cavity length  $L$ , i.e., the distance between the two cavity mirrors, to the length  $L_A$  over which the absorber is present (in our case the overlap of photolysis beam and absorption path),  $c$  is the light speed. One can either extract the absorption cross-section  $\sigma$  ( $\text{cm}^2 \text{ molecule}^{-1}$ ) for spectroscopic measurements or the concentration  $[A]$  ( $\text{molecules cm}^{-3}$ ) of the target molecule for kinetic experiments. This treatment implies that the concentration of the absorbing species does not change on the timescale of a ring-down event: this can be safely assumed in our experiments, since the ring-down time is on the order of a few  $\mu\text{s}$  (typically  $6 \mu\text{s}$  for the empty cavity), while the kinetics decay on the msec timescale. Note that experimental schemes have been developed taking advantage of the kinetic decays faster than the ring-down events [32, 33].

Compared to conventional absorption techniques, CRDS provides the advantage of being insensitive to power source fluctuations. Our ring-down cavity is set-up by two low loss mirrors (Layertec –  $99.95\% < R < 99.97\%$  –  $d = 7.75$  mm) separated by 78 cm leading to a 192 MHz free spectral range ( $\text{FSR} = c/2L$ ) for a few tens of Hz modewidth and ring-down times of  $\tau_0 = 5$ – $10 \mu\text{s}$ . These numbers bring to light mode-matching issues since the needed resonance condition is obtained only when one of the cavity modes overlap with the emitted laser line. Two main methods are explored to achieve that requirement: the first is to use a pulsed laser [34] by-passing the mode-matching problem thanks to a spectral linewidth larger than a FSR which thus excites several cavity

modes. The use of narrower bandwidth continuous lasers requires an active scheme to couple with high-finesse cavities. Several versions to perform cw-CRDS have been developed over the last ten years, presenting different performances and complexity levels [30, 35–39]. We chose to use one of the less experimentally demanding schemes, first presented by Romanini et al. [40] in 1997.

As depicted in Fig. 1 and described in Sect. 2.1, the cavity was designed to overlap the photolyzed volume on a maximized distance of  $L_A$ . One cavity mirror is mounted on a piezo-electric transducer (P-305.00, Physic Instrumente) in order to modulate the cavity length with a triangular signal. The amplitude of this signal is set slightly higher than the free spectral range to achieve the resonance requirement twice per period (see the signals (a) and (b) in Fig. 2). A near-infrared beam, provided by a fibered distributed feedback (DFB) diode laser (Fitel–Furukawa), is coupled into the cavity through a set of lenses and mirrors in order to obtain a good cavity mode matching to excite the fundamental TEM<sub>00</sub> modes. The beam passes through an optical isolator and an acousto-optical modulator (Gooch and Housego-M040) allowing one to deviate the laser beam with a delay of 350 ns, with respect to the trigger signal. The first-order beam is directed into the cavity, while the non-deviated zero order beam is injected into the fibered entrance of a wavemeter (Burleigh WA-1100), allowing one to monitor periodically the diode laser emission wavelength. The optical signal transmitted through the cavity is converted into current by an avalanche effect photodiode (Perkin Elmer, C30662E)

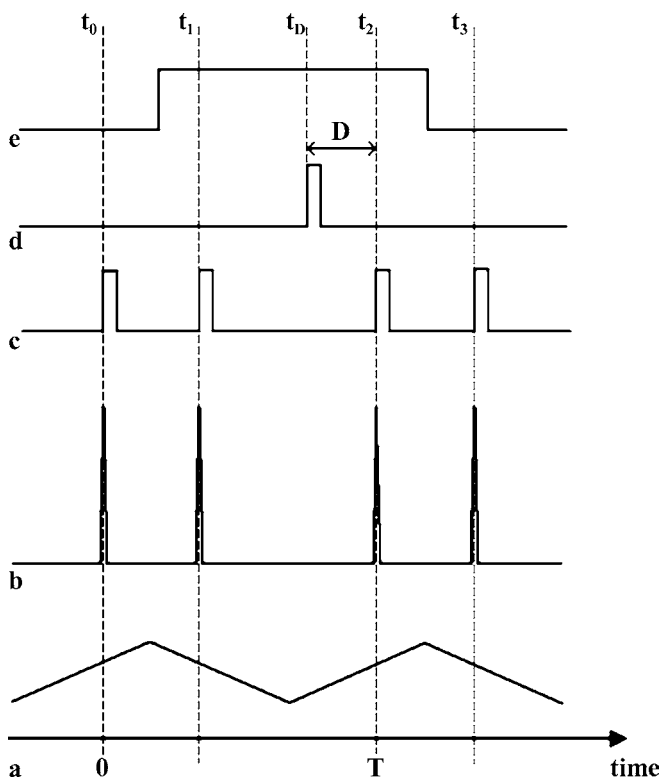


**FIGURE 2** Timing scheme for spectroscopic measurements. (a) triangular voltage applied to piezoelectric transducer (b) cavity modes recorded by the photodiode (c) ring-down trigger pulses (d) photolysis trigger pulse (e) recording time window

providing a responsivity of  $9.5 \text{ A W}^{-1}$  at 1550 nm. A home-made amplifier-threshold circuit converts the current signal to an exploitable voltage signal and triggers the acousto-optical modulator, the delay generator (Princeton Applied Research, Model 9650) and to the oscilloscope (TDS 5052, Tektronix). The entire detection system has a bandwidth of 5 MHz.

A personal computer is linked to the main devices either by general purpose interface bus (PCI-GPIB Interface Card, National Instruments) or by BNC wires (Data Acquisition Board PCI-6221, National Instruments). Control of the experiment and the data processing are executed by a Labview 7.1 program. In this way, each waveform recorded by the oscilloscope is entirely transferred to the computer and the ring-down events are extracted from this signal. The individual decays, sampled into a  $40 \mu\text{s}$  time window with 400 or 800 ns time resolution, are fitted by a Levenberg-Marquardt Labview Virtual Instrument.

### 2.3 Timing strategies

One of the advantages of pulsed CRDS compared to cw-CRDS is its easy timing control making it very suitable for pump-probe experiment [17–24], using cw diode lasers implies more difficult timing control. In order to monitor the HO<sub>2</sub> radical using cw-CRDS, we have used two different timing strategies for either spectroscopic or kinetic experiments.

**2.3.1 Timing scheme for spectroscopic measurements.** As HO<sub>2</sub> has a short lifetime, recording its spectrum requires us to detect it very quickly after the photolysis pulse in order to get a strong absorption signal (Fig. 6). Figure 2 shows the signals involved in the trigger scheme. Since modulating the cavity length periodically fulfils the resonance condition, we use this time relation to predict when ring-down events will occur, as shown by signals (a) and (b): two events are obtained per modulation period  $T$ , one on the positive slope at  $t_0$ , the other on the negative slope at  $t_1$ . The interval between these two events is governed by the offset of the modulation signal and by slow mechanical drifts of the mirror position, so it seems difficult to predict the ring-down event at  $t_1$  relative to the one at  $t_0$ . The interval between  $t_0$  and  $t_2$  on the other hand is, besides the jitter, equal to the modulation period  $T$ . This enables us to get the wanted delay  $D$  by triggering the photolysis pulse (d) at the time  $t_D = T - D$ . In order to acquire the spectrum baseline and the HO<sub>2</sub> absorption signal, we start a 20 ms recording time window 18 ms before the photolysis pulse and thus obtain one (or more) ring-down event before the pulse and, in general, one other within 2 ms after. The ring-down events are extracted from the 20 ms time window and analyzed the same way as described in the next paragraph. Typically eight events occurring after the photolysis pulse are averaged before going on to the next wavelength step. Using this acquisition protocol, we obtain a scan speed of approximately  $0.6 \text{ cm}^{-1} \text{ h}^{-1}$  for a  $0.003 \text{ cm}^{-1}$  wavelength resolution.

**2.3.2 Timing scheme for kinetic measurements.** In order to measure the rate constants of reactions involving the HO<sub>2</sub> radical, one needs to monitor its concentration over a period of several milliseconds after the photolysis pulse. The recording

time window, in general is 40 ms, is triggered a few milliseconds before the excimer pulse in order to get  $\tau_0$  and the  $\text{HO}_2$  absorption signal  $\tau$  at each photolysis pulse. The acquisition rate (number of ring-down events acquired per shot) is directly linked to the cavity length frequency modulation and to the recording window duration, being only limited by the laser diode power: the higher the modulation frequency, the worse the cavity injection efficiency [41], i.e., increasing the triangular voltage frequency applied to the piezoelectric transducer decreases the light build-up intensity in the cavity. The chosen frequency value (between 50 and 500 Hz) is thus a compromise between a good acquisition rate and allowing the exciting  $\text{TEM}_{00}$  modes to become intense enough to activate the trigger circuit: at typical frequencies of 100 Hz, eight ring-down events will be observed in the 40 ms time window.

The signal from the photodiode is recorded on channel 1 of the oscilloscope, while the signal from the trigger circuit is recorded on channel 2, with a maximal resolution of 100 000 points on each channel (i.e., 400 ns/points for a 40 ms time window). After every excimer laser pulse, both traces are transferred to the personal computer, where the data are treated by the Labview routine: first the trigger signals are searched on trace 2, and then, with knowledge of the delays, the ring-down signals are recovered from trace 1 as a 40  $\mu\text{s}$  time window. Thereafter, the ring-down signals are treated as describes above, i.e., a fit is executed over 40  $\mu\text{s}$ , starting shortly after the trigger signal (the time frame omitted for the fitting procedure, is fixed by the operator and covers in general the first 1 to 3 data points, i.e., 0.4 to 1.2  $\mu\text{s}$ ). The residual returned by the fit procedure is compared to a threshold, fixed by the operator, and only after passing this test, the ring-down time is saved together with the delay time obtained from trace 2. The entire procedure takes up to 6 s, depending on the number of events to be fitted, i.e., the frequency applied to the piezoelectric transducer.

To finish this section, we introduce the jitter that influences the timing control. We can distinguish the delay fluctuations due to environmental perturbations (e.g., pumping

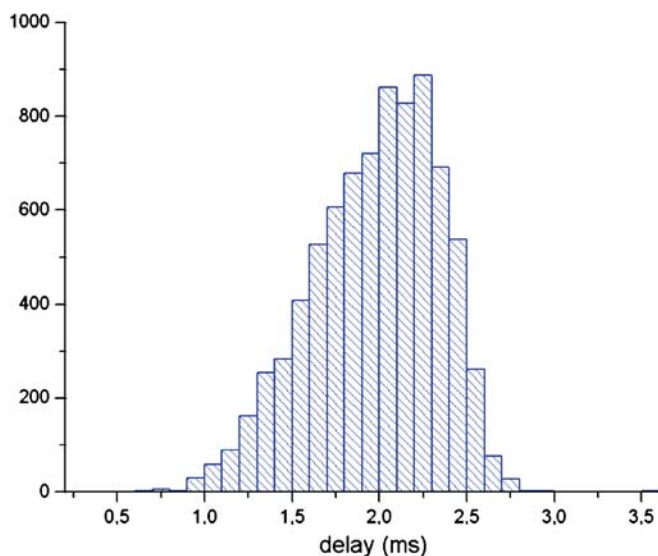
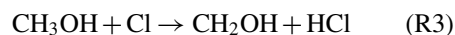


**FIGURE 3** Distribution of the delays for a total of 8005 events, predicted to occur at  $t_D = 2$  ms: nearly all events fall into a 2 ms time window

vibrations, thermal drifts) from the jitter caused by the diode laser emission. As described recently [42], the laser phase noise brings us to consider instantaneous laser frequency fluctuating inside the laser linewidth. The high-finesse cavity converts these frequency fluctuations into amplitude fluctuations; the instantaneous laser frequency leading to resonance conditions. Consequently, these amplitude fluctuations recorded by the photodiode induce jittering of the ring-down events since the trigger circuit has to reach a fixed amplitude value to switch the AOM. As can be seen in Fig. 3, typical delay fluctuations affecting our experiment are around 2 ms. This is good enough for spectroscopic measurements, i.e., most of the photolysis pulses will generate a ring-down event within the 2 ms window, while for kinetic experiments the jitter helps to spread the delay of the ring-down events around the cavity modes (see Fig. 4).

### 3 Results and discussion

$\text{HO}_2$  radicals have been generated by laser flash photolysis (Lambda Physic LPX 202i) of  $\text{SOCl}_2$  at 248 nm in the presence of  $\text{CH}_3\text{OH}$  and  $\text{O}_2$



Typical experimental conditions were  $[\text{SOCl}_2]_0 = 1\text{--}2 \times 10^{14} \text{ cm}^{-3}$ , which translates with our average photolysis power of 400 mJ/pulse into  $[\text{Cl}]_0 = 5\text{--}10 \times 10^{13} \text{ cm}^{-3}$ .

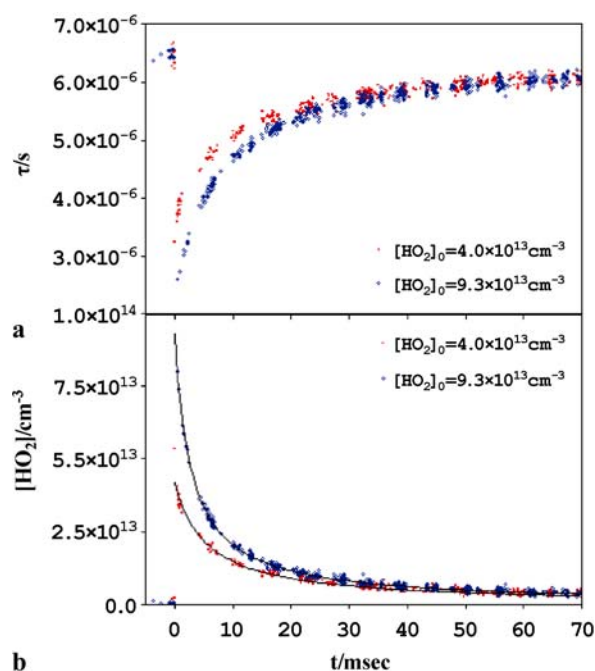
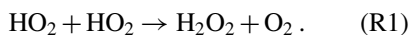


**FIGURE 4** (a) Time-resolved cavity ring-down time for two different  $[\text{HO}_2]$ : each dot corresponds to one ring-down event at a delay  $t$  with respect to the photolysis pulse at  $t = 0$  ms. The events cluster more or less at the cavity modes. Typically 500 events are recorded for each  $[\text{HO}_2]$ , measuring time is 3–5 min with  $\approx 10$  events per photolysis pulse and 0.5 Hz repetition rate (b) Above signals transformed in absolute  $\text{HO}_2$  concentrations, full line is the model with  $k_1$  as given in the text

Typical initial CH<sub>3</sub>OH and O<sub>2</sub> concentrations have been  $1 \times 10^{16}$  and  $5 \times 10^{16} \text{ cm}^{-3}$ , respectively. Using the well-known rate constants for (R3) [43] and (R4) [44], Cl-atoms are converted under these conditions to HO<sub>2</sub> radicals within 10  $\mu\text{s}$  with a yield of 1. All experiments presented in this paper have been performed at a total pressure of 50 Torr of Helium.

### 3.1 Kinetic measurements

Absolute time-resolved HO<sub>2</sub> concentrations have been measured by cw-CRDS using the above described timing strategy. Raw data of a typical signal are shown in Fig. 4 for two different initial HO<sub>2</sub> concentrations: each dot represents the ring-down time  $\tau$  at a given delay with respect to the photolysis pulse. Under our experimental conditions, the HO<sub>2</sub> concentration decreases mainly through the well-studied self-reaction [1–4]



The HO<sub>2</sub> concentration-time profile is thus governed by the rate constant  $k_1$

$$\frac{1}{[\text{HO}_2]_t} = \frac{1}{[\text{HO}_2]_0} + 2k_1 t, \quad (3)$$

with  $[\text{HO}_2]_t$  being the radical concentration at time  $t$  and  $[\text{HO}_2]_0$  the initial peak radical concentration. A plot of  $[\text{HO}_2]^{-1} = f(t)$  should result in a straight line with a slope corresponding to  $2k_1$  and an intercept of  $1/[\text{HO}_2]_0$ . While the kinetic of this reaction has been the subject of many investigations, mainly by UV absorption spectroscopy [1–3], information on the near infrared spectroscopy of the HO<sub>2</sub> radical is sparse. We have, therefore, reversed the procedure and have deduced the HO<sub>2</sub> radical concentration and thus the absorption cross-section from the time-resolved absorption profile. Figure 5 shows the plot of

$$\frac{c}{R_L} \left( \frac{1}{\tau} - \frac{1}{\tau_0} \right) = \frac{1}{[\text{HO}_2]_0 \sigma_\lambda} = f(t). \quad (4)$$

The slope in these plots corresponds to  $2k_1/\sigma_\lambda$  while the intercept is equal to  $\sigma_\lambda/[\text{HO}_2]_0$ . The rate constant  $k_1$  is known to be enhanced by molecules like H<sub>2</sub>O, CH<sub>3</sub>OH or NH<sub>3</sub> [3, 45–48], but the concentrations used in our system are too low to become important ( $[\text{CH}_3\text{OH}] = 10^{16} \text{ cm}^{-3}$  leads to an enhancement of  $5.8 \times 10^{-14} \text{ cm}^3 \text{ s}^{-1}$  at 296 K [3]). For our purpose, we have, thus, adopted a value of  $k_{1,50 \text{ Torr}} = (1.9 \pm 0.2) \times 10^{-12} \text{ cm}^3 \text{ s}^{-1}$ , which is the average of the latest NASA recommendation [49] ( $k_{1,50 \text{ Torr}} = 1.77 \times 10^{-12} \text{ cm}^3 \text{ s}^{-1}$ ) and the recent study of Stone and Rowley [3] ( $k_{1,50 \text{ Torr}} = 2.07 \times 10^{-12} \text{ cm}^3 \text{ s}^{-1}$ ); this results in an absorption coefficients of  $(2.5 \pm 0.6) 10^{-19} \text{ cm}^2$  at 50 Torr for the transition at  $6625.784 \text{ cm}^{-1}$ . The given error reflects the uncertainty in the rate constant and an estimated uncertainty of 10% in the absorption pathlength, deduced only from pure geometrical calculations and not taking into account the divergence of the photolysis laser or the diffusion of the radicals out of the photolysis volume.

Bimolecular behavior of the concentration-time profiles have been observed over a large range of HO<sub>2</sub>-peak concentration, i.e., plots of (4) were linear over the entire concentration range and for long reaction times. It seems, therefore,

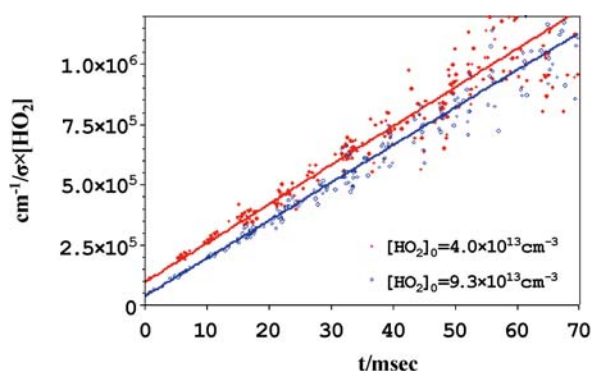


FIGURE 5 Plot of  $1/\sigma[\text{HO}_2]$  as a function of time for 2 different HO<sub>2</sub> concentrations. The slope of the linear regression is used to extract the absorption coefficient  $\sigma$

unlikely, that secondary reactions like the possible reaction of HO<sub>2</sub> with SOCl or a regeneration of Cl (and thus HO<sub>2</sub>) through a self reaction of SOCl influence significantly the HO<sub>2</sub> concentration-time profile. While a lot is known on the initial photodissociation of SOCl<sub>2</sub> [50–52], no information at all on the reactivity of SOCl radicals has been found in the literature; they probably form peroxy radical under our excess O<sub>2</sub> conditions which than could react with HO<sub>2</sub>. Note, that any secondary reaction removing HO<sub>2</sub> from the system would result in an apparently smaller absorption coefficient (the faster decrease in the concentration time profile asks for a higher initial  $[\text{HO}_2]$  concentration to fit the profile), while a regeneration of HO<sub>2</sub> through secondary reactions would result in a higher absorption coefficient.

A detection limit for our actual experimental set-up (mirrors with  $R = 0.9995$ ) of  $2 \times 10^{12} \text{ cm}^{-3}$  can be calculated for the absorption line at  $6625.784 \text{ cm}^{-1}$ , assuming a measurable decrease in ring-down time of 0.2  $\mu\text{s}$ . This detection limit will probably be decreased in future experiments thanks to mirrors with higher reflectivity (Los Gatos Research,  $R \geq 0.99995$ ).

### 3.2 Spectroscopic measurements

Figure 6 shows the time-resolved measurements of the absorption line at  $6625.784 \text{ cm}^{-1}$  at 50 Torr total pressure: kinetic decays over 40 ms have been recorded with a step width of  $0.003 \text{ cm}^{-1}$ . Individual decays have then been fitted with the rate constant  $k_1$  fixed to  $1.9 \times 10^{-12} \text{ cm}^3 \text{ s}^{-1}$ , leading to an initial concentration of  $[\text{HO}_2]_0 = 5 \times 10^{13} \text{ cm}^3$  and a peak absorption coefficient of  $2.5 \times 10^{-19} \text{ cm}^2$ . Figure 7 shows all absorption coefficients, obtained from the individual fits in Fig. 6, as a function of the wavelength. The full line represents a simple gaussian profile; pressure broadening is apparently not very important under these conditions (50 Torr He). The absorption line strength for this line has been obtained from the fit to  $S = (5.2 \pm 1.0) \times 10^{-21} \text{ cm}^2 \text{ molecule}^{-1} \text{ cm}^{-1}$  with a line width of  $0.017 \text{ cm}^{-1}$ . This can be compared to the only existing literature data of Johnson et al. [12] and Taatjes and Oh [14]: while Johnson et al. [12] reported a line strength of  $S = 1.6 \times 10^{-21} \text{ cm}^2 \text{ molecule}^{-1} \text{ cm}^{-1}$  for the strongest transitions in this wavelength range, Taatjes and Oh [14] reported a line strength of  $S = 2.4 \times 10^{-21} \text{ cm}^2 \text{ molecule}^{-1} \text{ cm}^{-1}$ . Johnson et al. have used the well known UV absorption at 220 nm to calibrate

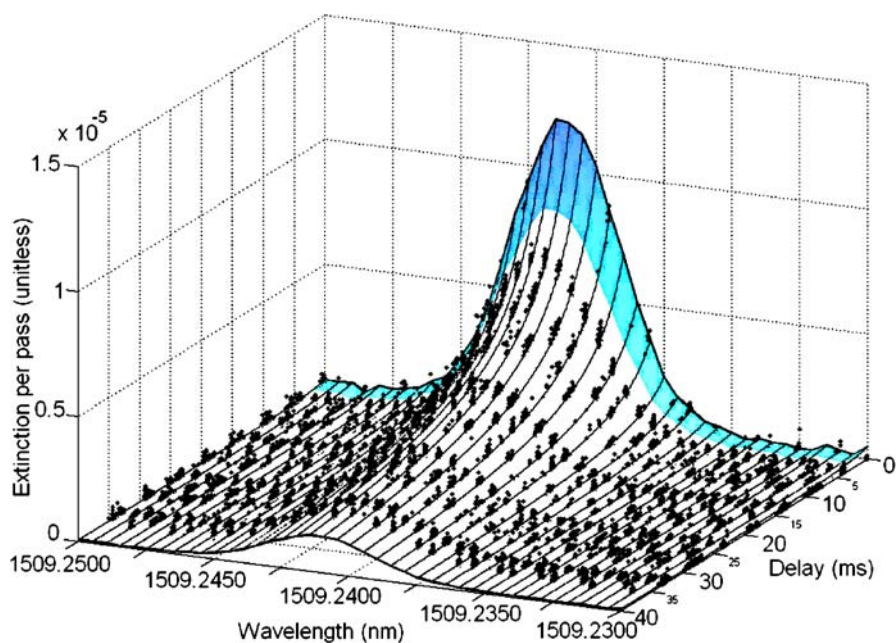


**FIGURE 6** Time-resolved absorption line of  $\text{HO}_2$ , decays for  $[\text{HO}_2]_0 = 5 \times 10^{13} \text{ cm}^{-3}$  have been monitored at different wavelength. For measuring the absorption spectra shown in Fig. 8, only ring-down events occurring 2 ms after the photolysis pulse, shown as blue shaded area, are taken into account

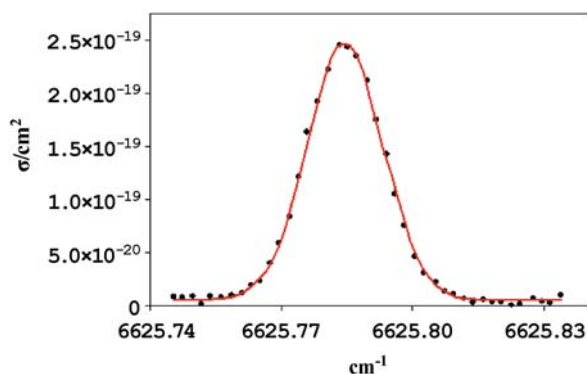


**FIGURE 7** Absorption line reconstituted from the fits shown in Fig. 6 at  $6625.784 \text{ cm}^{-1}$ : full line represents a Gaussian profile

their  $\text{HO}_2$  concentration, but also reported difficulties as stable diode laser emission and varying  $\text{HO}_2$  concentration. No details are given on the overlap of IR and UV absorption path. It is not clear, how the line strength reported by Taatjes and Oh [14] has been obtained, but they also report second order kinetics consistent with their line strength.

The most important error source in our experiment is the uncertainty in the chemistry, i.e., the fate of the  $\text{SOCl}_2$  radical. Nevertheless it appears difficult to imagine secondary reactions that would increase the apparent absorption coefficient by a factor of two and still deliver bimolecular concentration time profiles. It is, thus, not very clear what causes this important disagreement; future experiments are planned that will use  $\text{Cl}_2$  photolysis at 351 nm as radical source instead of  $\text{SOCl}_2$  in order to discover possible secondary reactions.

The blue-shaded area in Fig. 6 illustrates the time zone in which ring-down events are collected for spectroscopic measurements. Figure 8 shows the absorption spectra of  $\text{HO}_2$  in the wavelength range  $6625.2\text{--}6625.9 \text{ cm}^{-1}$ : the upper trace (a) shows the ring-down times before and after the photolysis pulse, each dot is the average of 8 events; the lower trace (b) has been converted to absorption cross-section relative to the line at  $6625.784 \text{ cm}^{-1}$ .

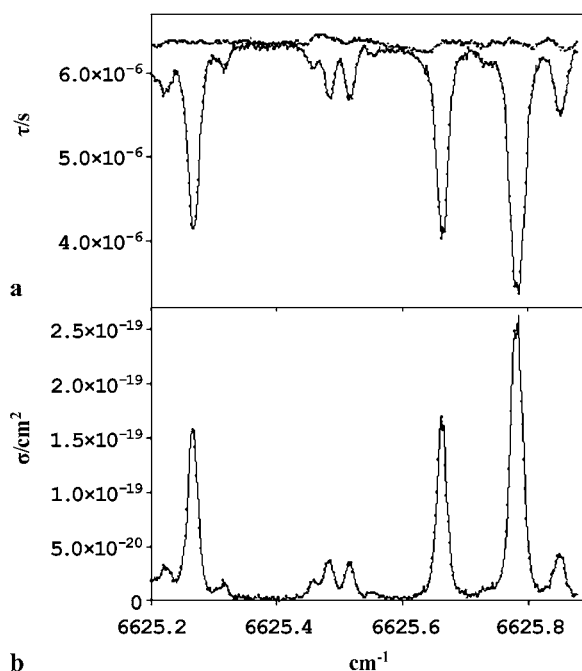


**FIGURE 8** Absorption spectra of  $\text{HO}_2$ , formed by photolysis of  $\text{SOCl}_2/\text{CH}_3\text{OH}/\text{O}_2$  in 50 Torr He. (a) The baseline consists of ring-down events occurring up to 18 ms before the photolysis pulse, the absorption takes into account events occurring up to 2 ms after the photolysis pulse. At each wavelength up to eight ring-down events are averaged. (b) Absorption spectrum, put on an absolute scale relative to the absorption cross-section of the line at  $6625.78 \text{ cm}^{-1}$ , calibrated through kinetic measurements

#### 4 Conclusion

We have presented in this paper a new experimental set-up allowing one to measure spectroscopic and kinetic data of reactive species absorbing in the near IR like the  $\text{HO}_2$  radical. Different timing strategies for obtaining kinetic or spectroscopic information have been developed and have been found more efficient than earlier set-ups [25]: decays over 40 ms can be measured within a few minutes with good

signal-to-noise ratio, absorption spectra with excellent signal-to-noise ratio can be acquired at a rate of 0.6 cm<sup>-1</sup>h<sup>-1</sup> with 0.003 cm<sup>-1</sup> resolution. The line strength of the absorption line at 6625.784 cm<sup>-1</sup> has been determined by means of the known rate constant of the HO<sub>2</sub>-self reaction to  $S = (5.2 \pm 1.0) \times 10^{-21}$  cm<sup>2</sup> molecule<sup>-1</sup>cm<sup>-1</sup>, which is two times more than earlier literature values.

**ACKNOWLEDGEMENTS** The authors are grateful to Daniele Romanini and Jérôme Morville for many helpful discussions and to Sabine Crunaire for practical help in many situations. This work is financially supported by the Nord/Pas de Calais region within the framework of the CPER, by the CNRS, the "Programme National de Chimie Atmosphérique" PNCA, the European funds for Regional Economic Development FEDER.

## REFERENCES

- 1 N. Kanno, K. Tonokura, A. Tezaki, M. Koshi, *J. Phys. Chem. A* **109**, 3153 (2005)
- 2 L.E. Christensen, M. Okumura, S.P. Sander, R.J. Salawitch, G.C. Toon, B. Sen, J.F. Blavier, K.W. Jucks, *Geophys. Res. Lett.* **29**, 1299 (2002)
- 3 D. Stone, D.M. Rowley, *Phys. Chem. Chem. Phys.* **7**, 2156 (2005)
- 4 R.S. Zhu, M.C. Lin, *Phys. Chem. Comm.* **23**, (2001)
- 5 A.A. Jemi-Alade, P.D. Lightfoot, R. Lesclaux, *Chem. Phys. Lett.* **195**, 25 (1992)
- 6 A. Tomas, E. Villenave, R. Lesclaux, *J. Phys. Chem. A* **105**, 3505 (2001)
- 7 M.E. Jenkin, R.A. Cox, G.D. Hayman, L.J. Whyte, *J. Chem. Soc. Faraday Trans. 2* **84**, 913 (1988)
- 8 O.J. Nielsen, M.S. Johnson, T.J. Wallington, L.K. Christensen, J. Platz, *Int. J. Chem. Kinet.* **34**, 283 (2002)
- 9 K.H. Becker, E.H. Fink, P. Langen, U. Schurath, *J. Chem. Phys.* **60**, 4623 (1974)
- 10 H.E. Hunziker, H.R. Wendt, *J. Chem. Phys.* **60**, 4622 (1974)
- 11 M.S. Zahniser, A.C. Stanton, *J. Chem. Phys.* **80**, 4951 (1984)
- 12 T.J. Johnson, F.G. Wienhold, J.P. Burrows, G.W. Harris, H. Burkhard, *J. Phys. Chem.* **95**, 6499 (1991)
- 13 E.H. Fink, D.A. Ramsay, *J. Mol. Spectrosc.* **185**, 304 (1997)
- 14 C.A. Taatjes, D.B. Oh, *Appl. Opt.* **36**, 5817 (1997)
- 15 L.E. Christensen, M. Okumura, S.P. Sander, R.R. Friedl, C.E. Miller, J.J. Sloan, *J. Phys. Chem. A* **108**, 80 (2004)
- 16 N. Kanno, K. Tonokura, A. Tezaki, M. Koshi, *J. Mol. Spectrosc.* **229**, 193 (2005)
- 17 L. Zhu, G. Johnston, *J. Phys. Chem.* **99**, 15114 (1995)
- 18 Y. Chen, L. Zhu, *J. Phys. Chem. A* **107**, 4643 (2003)
- 19 G.M.P. Just, E.N. Sharp, S.J. Zalyubovsky, T.A. Miller, *Chem. Phys. Lett.* **417**, 378 (2006)
- 20 S.J. Zalyubovsky, D. Wang, T.A. Miller, *Chem. Phys. Lett.* **335**, 298 (2001)
- 21 A.J. Huneycutt, R.N. Casaes, B.J. McCall, C.-Y. Chung, Y.-P. Lee, R.J. Saykally, *Chem. Phys. Chem.* **5**, 321 (2004)
- 22 F. Ito, T. Nakanaga, *Chem. Phys.* **277**, 163 (2002)
- 23 Y.M. Choi, W.S. Xia, J. Park, M.C. Lin, *J. Phys. Chem. A* **104**, 7030 (2000)
- 24 T. Yu, M.C. Lin, C.F. Melius, *Int. J. Chem. Kinet.* **26**, 1095 (1994)
- 25 D.B. Atkinson, J.L. Spillman, *J. Phys. Chem. A* **106**, 8891 (2002)
- 26 M. Hippler, M. Quack, *Chem. Phys. Lett.* **314**, 273 (1999)
- 27 C. Fittschen, A. Frenzel, K. Imrik, P. Devolder, *Int. J. Chem. Kinet.* **31**, 860 (1999)
- 28 M. Mazurenka, A.J. Orr-Ewing, R. Peverall, G.A.D. Ritchie, *Ann. Rep. Prog. Chem. C* **101**, 100 (2005)
- 29 B.A. Paldus, A.A. Kachanov, *Can. J. Phys.* **83**, 975 (2005)
- 30 G. Berden, R. Peeters, G. Meijer, *Int. Rev. Phys. Chem.* **19**, 565 (2000)
- 31 S.S. Brown, *Chem. Rev.* **103**, 5219 (2003)
- 32 S.S. Brown, A.R. Ravishankara, H. Stark, *J. Phys. Chem. A* **104**, 7044 (2000)
- 33 Y. Guo, M. Fikri, G. Friedrichs, F. Temps, *Phys. Chem. Chem. Phys.* **5**, 4622 (2003)
- 34 A. O'Keefe, D.A.G. Deacon, *Rev. Sci. Instrum.* **59**, 2544 (1988)
- 35 D.S. Baer, J.B. Paul, M. Gupta, A. O'Keefe, *Appl. Phys. B* **75**, 261 (2002)
- 36 S.M. Ball, R.L. Jones, *Chem. Rev.* **103**, 5239 (2003)
- 37 S.E. Fiedler, A. Hese, A.A. Ruth, *Chem. Phys. Lett.* **371**, 284 (2003)
- 38 T. von Lerber, M.W. Sigrist, *Chem. Phys. Lett.* **353**, 131 (2002)
- 39 G. Totschnig, D.S. Baer, J. Wang, F. Winter, H. Hofbauer, R.K. Hanson, *Appl. Opt.* **39**, 2009 (2000)
- 40 D. Romanini, A.A. Kachanov, N. Sadeghi, F. Stoeckel, *Chem. Phys. Lett.* **264**, 316 (1997)
- 41 J.W. Hahn, Y.S. Yoo, J.Y. Lee, J.W. Kim, H.-W. Lee, *Appl. Opt.* **38**, 1859 (1999)
- 42 J. Morville, D. Romanini, M. Chenevier, A. Kachanov, *Appl. Opt.* **41**, 6980 (2002)
- 43 G.S. Tyndall, J.J. Orlando, C.S. Kegley-Owen, T.J. Wallington, M.D. Hurley, *Int. J. Chem. Kinet.* **31**, 776 (1999)
- 44 W.B. DeMore, S.P. Sander, D.M. Golden, R.F. Hampson, M.J. Kurylo, C.J. Howard, A.R. Ravishankara, C.E. Kolb, M.J. Molina, *JPL Publication 97-4*, 1 (1997)
- 45 R.A. Cox, J.P. Burrows, *J. Phys. Chem.* **83**, 2560 (1979)
- 46 R.-R. Lii, M.C. Sauer, S. Gordon, *J. Phys. Chem.* **85**, 2833 (1981)
- 47 E.J. Hamilton, R.-R. Lii, *Int. J. Chem. Kinet.* **9**, 875 (1977)
- 48 R.S. Zhu, M.C. Lin, *Chem. Phys. Lett.* **354**, 217 (2002)
- 49 S.P. Sander, M.J. Kurylo, V.L. Orkin, D.M. Golden, R.E. Huie, B.J. Finlayson-Pitts, C.E. Kolb, M.J. Molina, R.R. Friedl, A.R. Ravishankara, G.K. Moortgat, *JPL Publication 02-25* (2003)
- 50 A. Chichinin, T.S. Einfeld, K.-H. Gericke, J. Grunenberg, C. Maul, L.V. Schäfer, *Phys. Chem. Chem. Phys.* **7**, 301 (2005)
- 51 M. Roth, C. Maul, K.-H. Gericke, *Phys. Chem. Chem. Phys.* **4**, 2932 (2002)
- 52 H. Wang, X. Chen, B.R. Weiner, *J. Phys. Chem.* **97**, 12260 (1993)